# Induction thermography: principle, applications and first steps towards standardization

by U. Netzelmann, G. Walle, S. Lugin, A. Ehlen, S. Bessert and B. Valeske

Fraunhofer Institute for Nondestructive Testing IZFP, University, Campus E3 1, Saarbruecken, Germany,
*udo.netzelmann@izfp.fraunhofer.de*

**Abstract**

A survey on theory, characteristic quantities and the experimental technique of induction thermography is given. The induction frequencies range from 1500Hz to 52MHz. Induction thermography is used for surface defect detection in forged parts of ferromagnetic steel. The sensitivity for crack detection is comparable to magnetic particle inspection. Hidden defects in steel can be detected, if necessary by lowering the induction frequency. Defects of fibres were detected in carbon fibre reinforced polymer. In silicon solar cells, cracks were detected with good contrast. A new field is crack detection in railway components like rails and wheels.

## 1. Introduction

Induction thermography or pulsed eddy current thermography uses electromagnetic pulses to excite eddy currents in electrically conductive materials. The eddy currents generate heat by resistive losses and release heat. The heat can be detected on the surface by an infrared camera. Surface cracks or hidden cracks close to the surface cause local changes of the electrical current densities, which become visible in the thermographic images.

First applications in steel industry were reported more than two decades ago [1], where continuous inductive heating on moving steel bars was applied to detect longitudinal cracks. Further, the technique has been applied using periodic heating and phase sensitive detection for characterization of coating adhesion [2] and using pulsed excitation for crack detection in turbine blades [3]. New applications were reported on steel components and carbon fibre reinforced polymers [4]. There was significant work on analytical and numerical modelling of the signal from cracks [5,6]. The role of the current distributions was studied [7]. Recent applications were devoted to testing of adhesive bonds [8] and describe carbon fibre laminate testing [9].

In this contribution, first, the characteristic electric and thermal quantities will be discussed. Then examples will be shown for different application fields of induction thermography. Extension of the frequency range to very low and very high frequencies is a major point. A final remark is given to the present efforts for standardization of induction thermography.

## 2. Materials and characteristic lengths

In contrast to eddy current testing, induction thermography has both an electromagnetic and a thermal aspect [10]. In order to the estimate the ability to detect defects in materials by induction thermography, one has to consider the electromagnetic skin depth, which describes the depth of the induction current flow. It is given by

$$\sigma_e = \sqrt{\frac{1}{\pi f \sigma_e \mu}} \,, \tag{1}$$

where $\sigma_e$ is the electrical conductivity, $\mu$ the magnetic permeability and $f$ is the electromagnetic frequency. According to Joule´s heating law the characteristic length for induction heating is half of the electromagnetic skin depth.

Another characteristic length is the thermal penetration depth $\mu_T$. The depth of the thermal propagation for a given observation time $t_{obs}$ (in a pulsed experiment) or modulation frequency $f_{mod}$ (in a periodically modulated experiment), is given by $\mu_T = 2\sqrt{\alpha t_{obs}}$ or $\mu_T = \sqrt{\frac{\alpha}{\pi f_{mod}}}$ , respectively. The latter is called thermal diffusion length.

Here, $\alpha$ is the thermal diffusivity of the material. Table 1 lists some materials and typical values for an induction frequency of $f$=100kHz and an observation time $t_{obs}$=100ms.

*Table 1.* Material parameters and characteristic lengths

| group | | electrical conductivity in $10^6$ S/m | relative magnetic permeability | thermal diffusivity in $10^{-6}$ m²/s | electromagnetic skin depth in mm (100 kHz) | thermal penetration depth in mm (t=0.1 s) |
|---|---|---|---|---|---|---|
| I | cast iron | 6.2 | 200 | 14.9 | 0.045 | 2.44 |
| | nickel, pure | 14.62 | 100 | 22.9 | 0.042 | 3.03 |
| II | silver, pure | 62.87 | 1 | 173 | 0.201 | 8.32 |
| | zinc, rolled | 16.24 | 1 | 41.2 | 0.395 | 4.06 |
| | aluminium 2014-T6 | 22.53 | 1 | 73 | 0.335 | 5.40 |
| | copper, pure | 60.09 | 1 | 112 | 0.205 | 6.71 |
| III | Inconel 600 | 0.98 | 1 | 3.13 | 1.608 | 1.12 |
| | stainless steel 316 | 1.33 | 1 | 7.09 | 1.380 | 1.68 |
| | titanium 6AL-4V | 0.58 | 1 | 6.59 | 2.090 | 1.62 |
| IV | carbon fiber reinforced polymer | 0.001 | 1 | 3.65 | 50 | 1.21 |
| | SiC Ceramic | 0.00005-0.001 | 1 | 22 | 50-225 | 2.97 |
| | Silicon | 0.001 | 1 | 89.2 | 50 | 5.97 |

Four groups of materials can be identified in table 1. Due to their high magnetic permeability, the ferromagnetic metals (group I) have a very small skin depth compared to the thermal penetration. Only a thin surface layer generates the heat. The non-magnetic metals in group II are often good electrical conductors, but their relative permeability is close to one. Their skin depth is still one order below the thermal penetration. In group III one can find metallic alloys with relatively poor electrical and thermal conduction, like Inconel or stainless steel. Here, the electromagnetic and thermal penetration depth are of comparable size for the given parameters. Finally, the materials of group IV have an electromagnetic skin depth significantly larger than the thermal penetration.

Defects that are deeper than the electromagnetic skin depth can still interact thermally with the heat generated at the surface of the test object, if there are obstacles to the heat flow into the depth of the material. Defects within the electromagnetic skin depth, that do not interact with the induction currents may still interact thermally. In total, a large class of defects within a depth smaller than $\delta_e$ or $\mu_T$ can be detected.

## 3. Experimental

A typical experimental setup is shown in figure 1. A high frequency induction coil in the neighbourhood of the test object generates eddy currents in pulses of typically 50 to 500ms length. The infrared camera records the surface radiation from shortly before until some time after the heating pulse. Another possibility, in particular when the available maximum induction power is low, is amplitude modulation of the high-frequency signal at lower modulation frequencies $f_{mod}$. Then, a lock-in algorithm is applied to the recorded image sequence in order to calculate an amplitude and a phase image [4]. Camera, induction coil ant test object can also be in relative movement. The third possibility to introduce time-dependent heat flows is to move a permanent magnet with sufficient relative speed to the test object. This will induce eddy currents that generate heat (principle of the eddy-current brake) [11].
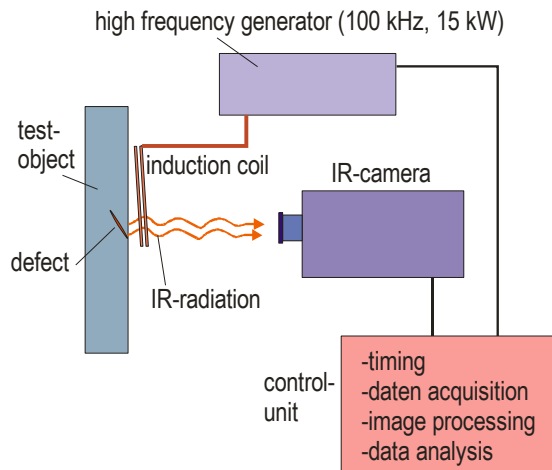
high frequency generator (100 kHz, 15 kW)

test-object

induction coil

IR-camera

defect

IR-radiation

control-unit

-timing
-daten acquisition
-image processing
-data analysis

**Fig. 1.** *Scheme of a set-up for induction thermography*

The induction coils used can be similar to those used for induction hardening or other industrial heating tasks. They can be air coils with or without water cooling. Helmholtz coils were reported, that have the advantage to homogenize the excitation field and to allow full optical access to the component surface for the infrared camera [12]. The magnetic flux of a coil can also be concentrated by using a yoke made out of a material with high permeability. Covering the metal of the coil by a thermally thick insulator helps to reduce time-dependent thermal radiation from the coil.

It can be shown, that the absorbed power density S into an electromagnetically thick material is given by

$$S = \frac{1}{2\mu_0^{\,2}} b^{\sim 2} \sqrt{\frac{\pi\mu_0\mu_R}{\sigma_e} f} \; , \qquad (2)$$

where $b^\sim$ is the high-frequency magnetic field, $\mu_0$ the permeability constant, $\mu_R$ the active effective magnetic permeability [13]. It can be noted, that S increases with the square root of the induction frequency, which favors the use of higher induction frequencies, if the excitation field can be maintained. A higher permeability helps to increase the signal, which explains the good efficiency of induction thermography for testing ferritic steel. For magnetic materials, equation (2) is an approximation for small deviations of the magnetization from its equilibrium. It has been shown, that static magnetic fields applied in addition to the high-frequency field can improve the thermographic contrast of cracks, when applied in the right direction [13].

## 4. Applications

### 4.1. Forged and hardened components

The standard NDT technique for testing components made out of ferritic steel is magnetic particle testing (MT). These inspections are usually performed by human operators in test cabins under UV light. In the automotive field, parts are usually manufactured in mass production. Therefore, in this industrial branch there is big interest for fast, automated NDT solutions without the necessity to apply liquids and chemical agents to the object surfaces.

A previous study [10] has shown that typical cracks occurring in forged parts can be detected well by induction thermography. Detection limits for different types of surface cracks were determined. There was also a first reliability study that indicated a good detection rate and low false alarm rate for induction thermography, whereas MT often suffers from a high number of false alarms.

In this and other studies [10,14], mainly pulsed high frequency bursts were used, which are probably the best approach, when the available testing time is small. Using periodically modulated high-frequency signals and lock-in processing, crack testing can be achieved at much lower excitation powers of some ten Watts or less [4]. The example shown in figure 2 was obtained at about 20W induction power with a measurement time of 3.5s. It can be seen that two radially oriented cracks are detected with a good contrast in the amplitude and the phase image. Contrasts on the conical surface due to reflection of external heat sources (bottom left image in figure 2) are suppressed by the lock-in calculation.

For forged ferritic steel parts it was shown that for small surface cracks, the signal contrast varies roughly with the product of crack length and crack depth, with some saturation towards very long and very deep cracks. Slanted cracks are even better detectable than cracks perpendicular to the surface, which favors detection of forging or rolling

laps. If the angle between crack direction and direction of the induced currents is varied from 90° to 0°, the thermal contrast decreases from 100% down to about 30%, which still allows detection with reduced S/N ratio.
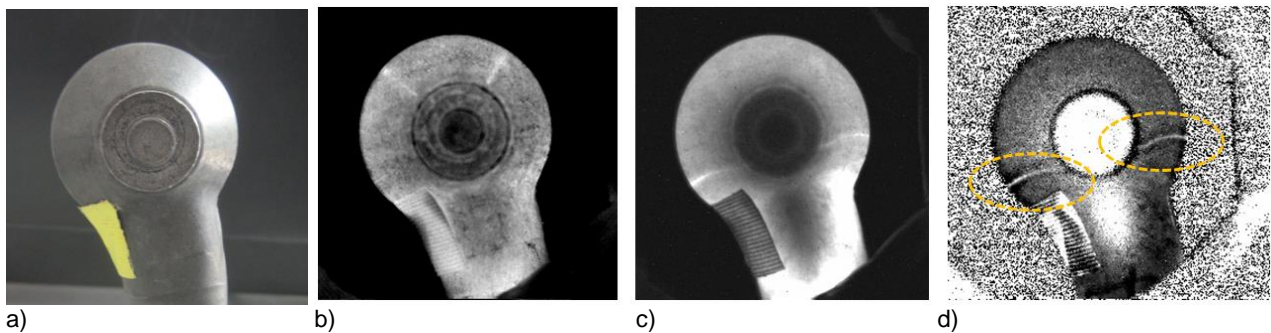


a)          b)          c)          d)

**Fig. 2.** *a): Photo of the forged part. b): passive infrared image, c): thermographic amplitude image at 4.5Hz, d) thermographic phase image at 4.5 Hz. Crack locations are marked.*

Another application demonstrates the detection of hardening cracks on a large gear-tooth (figure 3). The crack indication obtained by pulsed induction thermography is shown along with the conventional MT image as obtained under UV light. A concept for an automated manipulator was developed that scans all relevant faces of the test object.
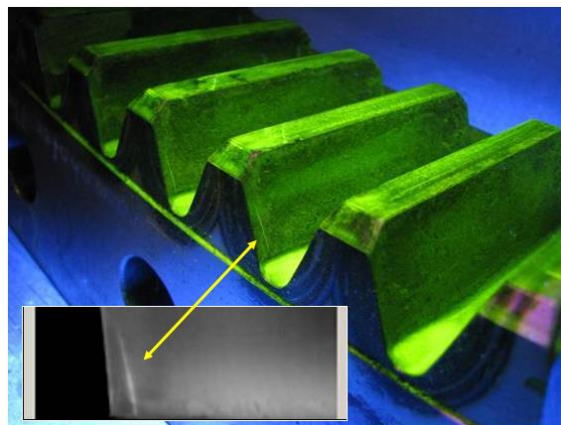


**Fig. 3.** *Hardening crack on a gear-tooth detected by induction thermography (small inset) and by magnetic particle testing (large picture)*

### 4.2. Hidden defects

A thermal contrast in induction thermography can be generated by electromagnetic interaction and/or by thermal interaction of the heat flow from the surface. If a hidden crack is deeper than the skin depth, it can still be detected by the thermal wave, if there is enough thermal interaction with the crack. For hidden cracks perpendicular to the surface, this condition is not met. The only way to detect the crack by induction thermography is to enlarge the skin depth to at least half of the crack coverage. As a typical skin depth in ferritic steel is about 50 µm, low-frequency power induction generators are required to meet this condition for cracks with a coverage of some 100µm. Figure 4 shows thermographic images of a natural hidden crack with a distance to the surface of 140µm (as later verified by metallography, figure 4, right). At 100kHz induction frequency there is only a weak contrast. If the induction frequency is reduced to 1500Hz, there is sufficient electromagnetic interaction with the crack and a large crack contrast is obtained. The results are further supported by numerical simulation [15]. Frequencies down to 300Hz were used to detect hidden notches.
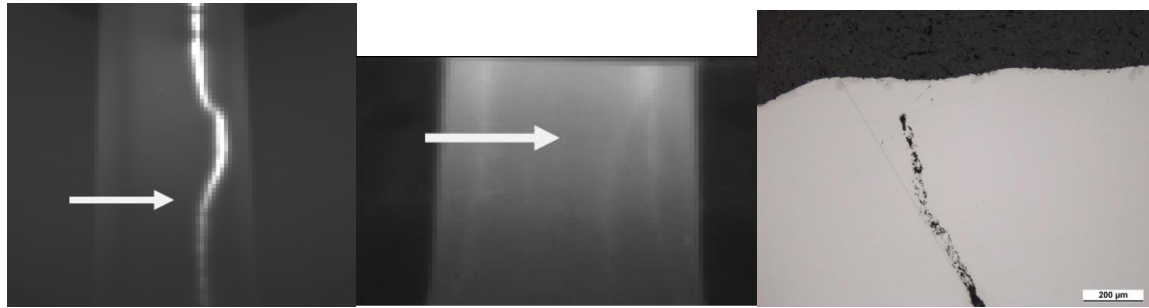
*Fig. 4. Left: Detection of a natural hidden crack in ferritic steel by induction thermography at 1500Hz excitation frequency. Middle: The same area imaged by induction thermography at 100kHz. Right: Metallographic cross-section along the arrow*

### 4.3. Carbon fibre reinforced polymer (CFRP)

Carbon fibre reinforced polymers are electrically conducting due to their content of carbon fibres. According to table 1, the skin depth at typical induction frequencies is about some centimeters. Therefore, components are often more of less homogeneously heated. Although the heating efficiency can be very good, flash thermography is often better to detect typical impact damage. Figure 5 shows a comparison. The impact damage is revealed clearly in the flash thermographic image. In the corresponding induction thermographic image, the contrast is dominated by the pattern of the carbon fibres in some proximity of the induction coil, which was located behind the CFRP plate. The induction frequency was about 250 kHz. The amplitude and the phase contrast obtained suggest, that inductive excitation detects predominantly the fibre damage and less the inner delaminations, which is understandable when considering the homogeneous heating over the plate thickness.
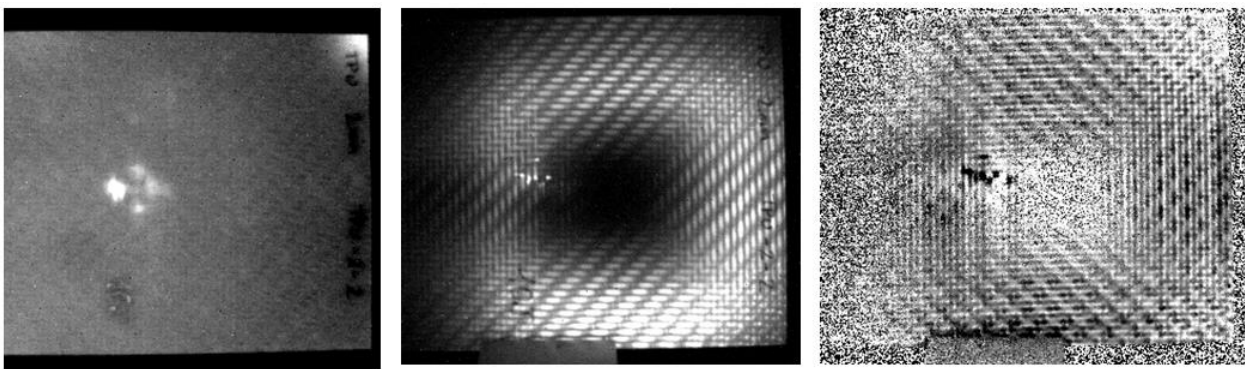


*Fig. 5. Left: Detection of an impact damage in CPRP by flash excited thermography. The same area was imaged by induction thermography with lock-in excitation. Middle: amplitude image. Right: phase image*

In order to detect delaminations and volume defects in CFRP by induction thermography, a possible way is to decrease the skin depth significantly. In the frequency range of some ten MHz, the skin depth should be reduced to the order of a mm. An induction system working with an antenna coil at 52MHz was developed. Results are shown in figure 6. The sample was a CFRP plate of 10mm thickness with a hole of 2mm diameter drilled into the end face. The distance from the hole to the top surface was 0.5mm. Due to limited available induction power at these frequencies, a lock-in technique was applied. Like in figure 5, the thermographic images are dominated by the pattern of the fibres. The signals are concentrated in direct proximity of the coil. In the phase image, a very weak contrast from the hidden hole below the surface can be detected. However, when compared to the contrast achieved by flash thermography, one has to recognize that the latter is the much better technique for this task [16].
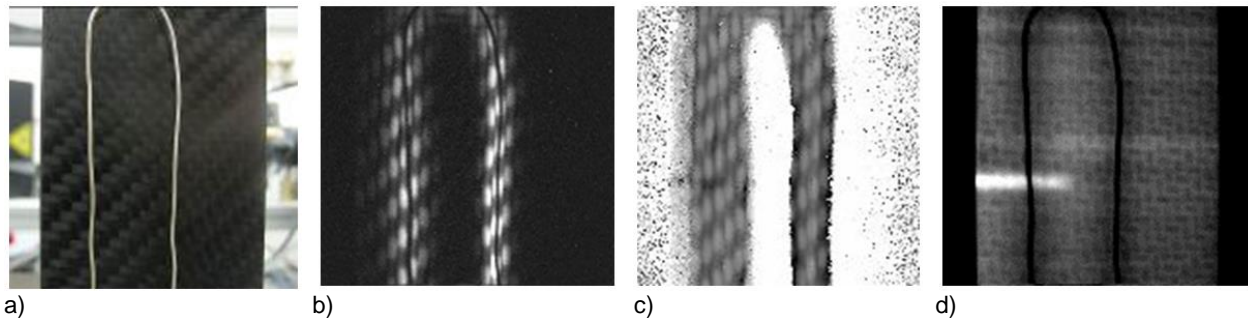
***Fig. 6.*** *a): Photo of the CFRP plate sample with induction coil. b) Thermographic amplitude image. c) Thermographic phase image. d) Flash excited thermography*

### 4.4. Solar cells

Thermographic techniques have proven to be very useful for characterization defects of different nature in solar cells [17]. Induction thermography can also be used for testing of solar cells, as silicon is a moderate electrical conductor. In contrary to CFRP, it is a good thermal conductor. One task is to detect cracks in the silicon in production processes. At usual induction frequencies, the electromagnetic skin depth is of the order of a few cm. Therefore currents are generated in the full volume of a typical cell. As silicon is quite transparent in the thermal infrared, the radiation detected is usually originating from the back-side metallization. Cracks in the brittle material can be long, but they are visually difficult to recognize. Currents that were induced by a coil on the back-side of the cell have to circumvent the cracks and produce a rapidly decaying but strong thermal signal. For the measurement shown in figure 7, a 70ms long burst pulse at 180kHz was applied. The thermal image shows the crack accompanied by a thermal contrast, with a strong concentration around the crack tip [18].
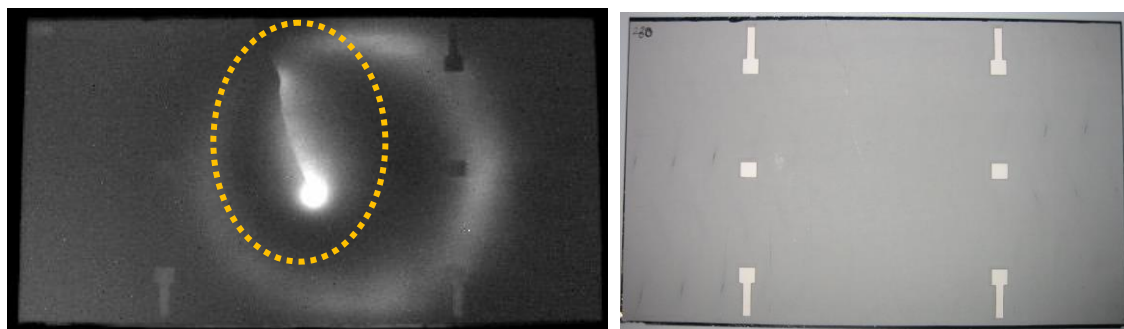


***Fig. 7.*** *Left: Thermographic image of a solar cell with crack (marked). Right: Photo back side of the solar cell*

### 4.5. Railway applications

#### 4.5.1. Rail surface defects

Since the railway accident in Hatfield, UK, in 2000 the effect of rail fatigue by rolling contact has received larger attention. In rails crack-like defects (e. g. squats) may occur, that are entering the rail head under a small angle. For rail testing, highly developed test cars equipped with ultrasound and eddy current devices have been in operation for some time. Within a European project there was the chance to use induction thermography to detect rail defects by inspection from a testing car in movement. A first preliminary experiment was performed on a German railway test site in July 2012.

After tests in the laboratory and simulation work, a measurement system for induction thermography was adapted for the application in the test car (figure 8). An infrared camera and an inductor were mounted under the car close to the rail surface. The induction generator was operated in cw permanent mode and therefore required water cooling. The induction generator and the cooling equipment as well as the data recording were located in the car.
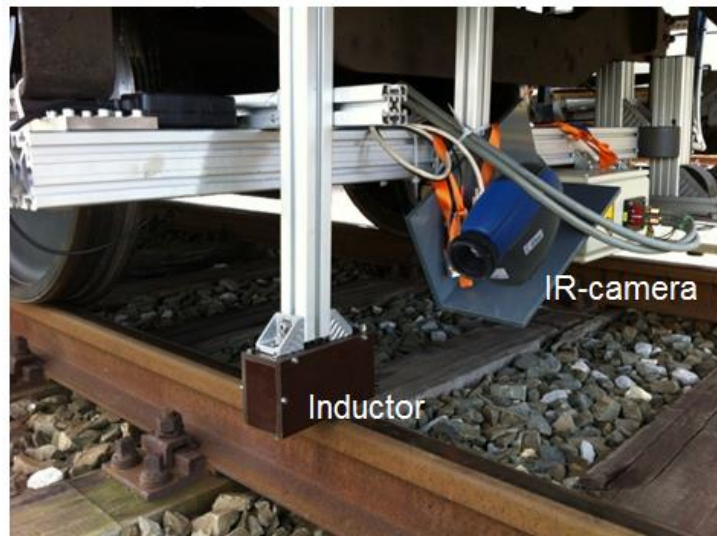
**Fig. 8.** *Thermographic set-up for rail surface defect testing mounted under a test car*

As the rails on the test site were in nearly perfect state, a part of a rail known to be defective was mounted parallel to the running rail in equal height and within a small distance. Inductor and camera were shifted aside correspondingly.

A thermographic indication for a defect of a natural crack-like surface defect is shown in figure 9. It was recorded at a test car speed of 2km/h. The thermal contrast from the crack can be seen clearly. Measurements were performed at different speed of the test train. The crack contrast decreased with train speed, but could be detected well up to a speed of 15km/h.
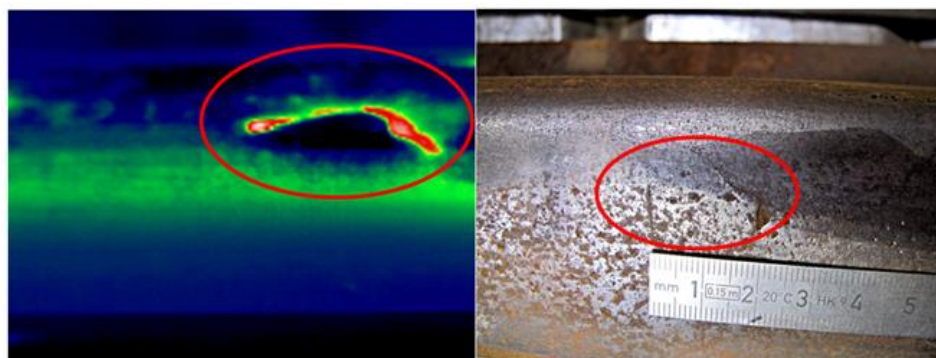


**Fig. 9.** *Left: Thermographic image of a rail surface defect obtained at a speed of 2km/h. Right: Photo of the defect area*

Advantages of induction thermography in comparison to the established techniques are that a defect image is generated by the camera, giving hints to the defect nature. No close contact of the inductor or the camera to the test object is needed. Defects can be detected in regions where other type of sensors fail due to geometrical restrictions.

### 4.5.2. Wheel surface defects

The flexibility of camera based solutions and the proven sensitivity of induction thermography to surface defects is also the basis for a demonstrator for thermographic crack detection on railway wheels, which is being set up in IZFP (figure 10). In connection with the infrared camera and the inductor moved by a robot, fully automated testing is performed. A proper combination of signal and image processing algorithms in connection with thermal post processing allows automated and robust defect detection. Beyond the possibilities of visual inspection, the time dependent thermal signals allow to obtain information on the defect depth. The technique works without application of coupling media or surface treatment.

***Fig. 10.*** *Demonstrator set-up for surface defect testing on railway wheels by induction thermography using a robot*

## 5. Standardization

Industry is interested to replace the well-established magnetic particle testing technique by a more objective technique suitable for automation. There is big interest on induction thermography. Up to now, however, introduction of this technique is impeded by missing standardization. The complex individual qualification by expertize or the validation are possible only at huge costs. In Fraunhofer IZFP, this route has been followed for induction thermography within its permit for flexible accreditation of new NDT techniques. Within the German research program „Transfer of R&D results by standardization" the project "InduNorm" was launched, that supports standardization activities and some research work still necessary for standardization. The project, which is ongoing at the time of writing, will also cover first proposals for standard test bodies.

## 6. Conclusion

Induction thermography can be applied to a wide range of materials that exhibit at least some electrical conductivity. Its ability to detect both surface cracks and hidden cracks close to the surface is very attractive, in particular for inspection of ferritic steel. The advantage of induction thermography compared to magnetic particle testing lies in the non-contact operation avoiding particle solutions and chemicals. Difficulties are occurring for application on highly reflecting aluminium alloys and other materials with highly reflecting surfaces and low emissivity. More pilot applications and standardization will increase the acceptance of the technique.

## REFERENCES

[1]  K.-J. Kremer, 'Das THERM-O-MATIC-Verfahren - Ein neuartiges Verfahren für die Online-Prüfung von Stahlerzeugnissen auf Oberflächenfehler', in: "3rd European Conference in Nondestructive Testing", Florence 15-18 October 1984, S. 171-186

[2]  D. M. Heath and W. P. Winfree, 'Quantitative thermal diffusivity imaging of disbonds in thermal protective coatings using inductive heating', Rev. Progr. Quant. Nondestr. Eval. **9**, D. O. Thompson and D. E. Chimenti (eds.), (Plenum Press New-York 1990), 577-584

[3]  J. Bamberg, G. Erbeck, G. Zenzinger, 'Eddy-Therm: Ein Verfahren zur bildgebenden Prüfung metallischer Bauteile', ZfP-Zeitung 68 (1999) 60-62Pradere C., Joanicot M., Batsale J-C., Toutain J., Gourdon C.,

[4]  G. Riegert, T. Zweschper, G. Busse, 'Lockin thermography with eddy current excitation', QIRT Journal **1** (2004) 21-32

[5]  B. Oswald-Tranta, 'Thermoinductive investigations of magnetic materials for surface cracks', QIRT Journal **1** (2004) 33-46

[6]  G. Walle, U. Netzelmann, 'Thermographic Crack Detection in Ferritic Steel Components Using Inductive Heating', Proc. 9th ECNDT Berlin, 25.-29.9.2006, DGZfP Berichtsband BB **103**-CD, Paper Tu.4.8.5

[7]  J. Vrana, M. Goldammer, J. Baumann, M. Rothenfusser, W. Arnold: 'Mechanisms and Models for Crack Detection with Induction Thermography', Review of progress in quantitative nondestructive evaluation 27, AIP Conference Proceedings **975** (2008) 475-482

[8]  L. Balaji, K. Balasubramanian, and C. Krishnamurty, 'Induction thermography for non-destructive evaluation of adhesive bonds', Proc. 39th RQNDE, AIP conf. proc. **1511**, (2013) 579-586

[9]  Y. He, G. Tian, M. Pan and D. Chen, 'Impact evaluation in carbon fiber reinforced plastic (CFRP) laminates using eddy current thermography', Composite Structures **109** (2014), 1-7

[10] U. Netzelmann and G. Walle, 'Induction Thermography as a Tool for Reliable Detection of Surface Defects in Forged Components', Proc. 17th World Conference on Nondestructive Testing, 25-28 Oct 2008, Shanghai, China

[11] German Patent DE102006050025B3

[12] J. Wilson, G. Tian, I. Abidin, S. Yang, and D. Almond, 2010. 'Pulsed eddy current thermography: system development and evaluation', Insight: Non-Destructive Testing and Condition Monitoring **52** (2010) 87-90

[13] P. Jäckel and U. Netzelmann, 'The influence of external magnetic fields on crack contrast in magnetic steel detected by induction thermography', QIRT Journal **10** (2013) 237-247

[14] P. Bouteille and G. Legros, 'Induction thermography as an alternative to conventional NDT methods for forged parts', Proc. QIRT 2014, Bordeaux, QIRT open archives QIRT-2014-134

[15] G. Walle, U. Netzelmann, C. Stumm and B. Valeske, 'Low frequency induction thermography for the characterization of hidden cracks in ferromagnetic steel components', Proc. 11th Int. Conf. on Quantitative Infrared Thermography (QIRT), 11.-14.6.2012, Naples, Italy, paper 218, ISBN 9788890648441

[16] M. Rothenfusser, U. Netzelmann (Hrsg.), 'Optische Mess- und Prüftechniken im infraroten Spektralbereich für den Einsatz in der Produktentwicklung, der Produktion und im Service: Ergebnisbericht des BMBF Verbundprojektes InfraSpek', München [u. a.] (2011)

[17] O. Breitenstein, J. Rakotoniaina, and M. Al Rifai, 'Quantitative Evaluation of Shunts in Solar Cells by Lock-in Thermography', Prog. Photovolt: Res. Appl. **11** (2003), 515-526

[18] U. Netzelmann, 'Thermographische Prüfung von Solarzellen auf Risse und Kontaktierungsfehler', DGZfP Jahrestagung 2014, Potsdam, DGZfP Berichtsband BB **148**-CD – Di.3.C.1